Optimized FDTD Schemes for 3D Acoustic Wave Propagation

Optimized FDTD Schemes for 3-D Acoustic Wave Propagation

Stefan Bilbao

***Abstract*—Finite difference time-domain simulation methods in acoustics applications have seen increased interest recently. The simplest scheme exhibits various weaknesses, such as numerical dispersion and anisotropy. More general parameterized families of schemes are explored here, with a view towards reducing such numerical artefacts through optimization. Numerical results are presented.**

***Index Terms*—Finite difference schemes, finite difference time-domain (FDTD) method, room modeling.**

I. Introduction

In spatial audio rendering applications (such as, e.g., artificial reverberation, or concert hall design), full wave-based modeling techniques are seeing increasing interest. Such brute force methods, in contrast to those based on simplifications such as ray tracing [1], or image source techniques [2], allow a complete rendering of the acoustic field anywhere within an enclosure. Various techniques have emerged—probably the best-known are finite difference time-domain (FDTD) methods [3], [4], which are intimately related to (and ultimately equivalent to) digital waveguide meshes [5], [6], which have seen much development, resulting in a full 3-D rendering system for low frequency acoustics [7]. Such low-frequency methods are often hybridized with ray-based methods [8]. An obvious (and unavoidable) downside of such full 3-D modeling is that it is computationally intensive, requiring, even for moderately-size rooms and at audio sample rates, a very large computational overhead.

The majority of the work on time-stepping methods has concentrated on schemes which operate over regular Cartesian grids. Probably best known is the simple scheme, where updating is carried out, at a given grid point, through accesses to previously computed values at the six neighboring points [9]. As is well known, such a scheme exhibits severe numerical dispersion effects, seen in practice both as variation in wave speed with frequency, as well as with direction (anisotropy). It is thus worth exploring schemes which, while requiring greater computational overhead, allow more control over these undesirable artefacts—the greater computational costs of such schemes may be offset against the possibility of obtaining good quality results, even at low sample rates.

The 3-D wave equation is introduced in Section II, and a basic finite difference scheme is described in Section III. A parameterized family of schemes, geared towards reducing the effects of numerical dispersion and anisotropy, and requiring optimization strategies, is presented in Section IV. Numerical results appear in Section V.

Manuscript received August 04, 2011; revised November 16, 2011; accepted January 11, 2012. Date of publication February 03, 2012; date of current version April 03, 2012. The associate editor coordinating the review of this manuscript and approving it for publication was Mr. James Johnston.

S. Bilbao is with the Acoustics Group, University of Edinburgh, Edinburgh EH9 3JZ, U.K. (e-mail: sbilbao@staffmail.ed.ac.uk).

Digital Object Identifier 10.1109/TASL.2012.2186806

II. The 3-D Wave Equation

The usual starting point in linear models of acoustic wave propagation is the wave equation in 3-D:

$$\frac{\partial^2 w}{\partial t^2} = c^2 \Delta w, \qquad \Delta = \frac{\partial^2}{\partial x^2} + \frac{\partial^2}{\partial y^2} + \frac{\partial^2}{\partial z^2}. \tag{1}$$

Here, c is the wave speed, in m/s, t is a time variable, and $(x, y, z) \in \mathbb{R}^3$ are spatial coordinates, in m. The dependent variable $w = w(x, y, z, t)$ is often taken to be a pressure, but another choice is of a velocity potential [10].

System (1), defined over an unbounded space, is linear and lossless. As such, it is natural to examine wave-like solutions of the form

$$w(x, y, z, t) = e^{j(k_x x + k_y y + k_z z + \omega t)} \tag{2}$$

where $\mathbf{k} = [k_x, k_y, k_z]$ is a real-valued vector wavenumber, and ω is a real angular frequency. When inserted into (1), the following dispersion relation results:

$$\omega = c|\mathbf{k}|. \tag{3}$$

III. A Basic Finite Difference Scheme

In a finite difference framework, over a regular (Cartesian) grid, the solution $w(w, y, z, t)$ to (1) is approximated by a grid function $w^n_{l,m,p}$, representing an approximation to w at $x = lX$, $y = mX$ and $x = pX$, and $t = nT$, or integer l, m, p, and n. Here, X is the spacing between adjacent grid points, and T is the time step. $f_s = 1/T$ is the sample rate. In other mainstream simulation applications, there is often a premium placed on using larger time steps, in order to reduce computational complexity [11]. Here, however, no such freedom is possible—a scheme must operate at a certain rate in order to be able to adequately render the solution up to a given frequency.

The simplest possible scheme for the 3-D wave equation is standard, and may be written as follows:

$$\delta_{tt} w^n_{l,m,p} = c^2 \delta_{1,0,0} w^n_{l,m,p} \tag{4}$$

where the operators δ_{tt} and $\delta_{1,0,0}$ are an approximation to a second time derivative and a six-point approximation to the Laplacian respectively, defined as

$$\delta_{tt} w^n_{l,m,p} = \frac{1}{T^2}\left(w^{n+1}_{l,m,p} - 2w^n_{l,m,p} + w^{n-1}_{l,m,p}\right) \tag{5}$$

$$\begin{aligned}\delta_{1,0,0} w^n_{l,m,p} = \frac{1}{X^2}(&w^n_{l+1,m,p} + w^n_{l-1,m,p} \\ &+ w^n_{l,m+1,p} + w^n_{l,m-1,p} + w^n_{l,m,p+1} \\ &+ w^n_{l,m,p-1} - 6w^n_{l,m,p})\end{aligned} \tag{6}$$

where the notation $\delta_{1,0,0}$ will be clarified in Section IV-A.

A. Frequency Domain Analysis

In order to analyze this scheme, it is again useful to examine the behavior of a single traveling wave solution (through so-called von Neumann analysis [11]), sampled over a regular Cartesian grid, of the form

$$w^n_{l,m,p} = e^{j\left(n\omega T + lk_x X + mk_y X + pk_z X\right)}. \tag{7}$$

The numerical dispersion relation for the scheme is then

$$\sin^2\left(\frac{\omega T}{2}\right) = \frac{\lambda^2}{4}\hat{\alpha}_{1,0,0} \tag{8}$$

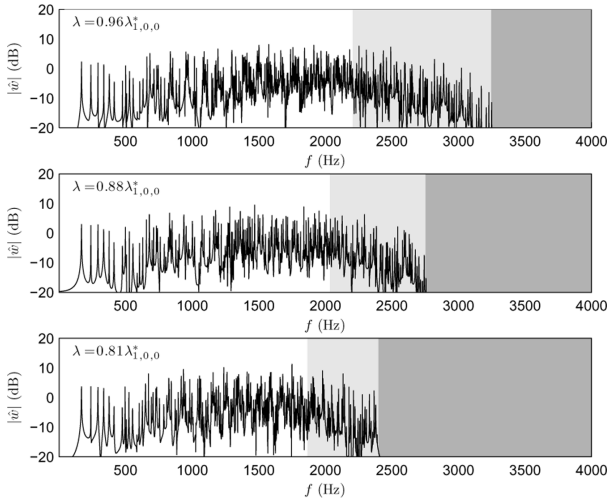

Fig. 1. Output spectra for the finite difference scheme (4) for the 3-D wave equation, for different values of λ, the Courant number. Here $c = 340$ m/s and the scheme operates at sample rate $f_s = 8$ kHz, over a cubic region, of side length 1 m. The scheme is excited with an impulse at time $t = 0$, at location $x = 0.21, y = 0.31, z = 0.71$, and output is read from location $x = 0.31, y = 0.81, z = 0.91$. For each value of λ, the dark shaded region corresponds to the frequency range above $f_{\max}$, where the scheme does not produce an oscillatory solution, and the light shaded range to the region above f_{trans}, where the modal density is incorrect.

where $\lambda = cT/X$ is the Courant number for the scheme, and where $\hat{\alpha}_{1,0,0}$ is defined as

$$\hat{\alpha}_{1,0,0}(\mathbf{k}X) = 2\left(3 - \cos(k_x X) - \cos(k_y X) - \cos(k_z X)\right). \quad (9)$$

Equation (8) is satisfied for real values of ω when

$$\lambda \leq \lambda^*_{1,0,0} = \frac{1}{\sqrt{3}} \quad (10)$$

which is a necessary stability condition for this scheme.

B. Cutoff Frequencies

For a given time step, if λ is held constant, then $X = cT/\lambda$, and it might seem that a choice of λ smaller than the bound given in (10) might be advantageous, in terms of efficiency, as the grid spacing becomes larger. In fact, this is not the case—such a choice leads to a numerical cutoff frequency.

To see this, note that the maximum frequency $\omega_{\max}$ (or frequency $f_{\max} = \omega_{\max}/2\pi$, in Hertz), for a given value of λ, will occur when the right-hand side of (8) is maximized—this value is given by

$$f_{\max} = \frac{\omega_{\max}}{2\pi} = \frac{1}{\pi T}\text{asin}\left(\sqrt{3}\lambda\right) \leq \frac{f_s}{2}. \quad (11)$$

There is thus a reduction in the available bandwidth of the scheme, as is easily observable in the plots in Fig. 1. This reduction is substantial, even for λ very near to $\lambda^*_{1,0,0}$. As a result, if one is interested in reducing computational complexity, a far better approach is to simply reduce the sample rate.

A more subtle transition frequency occurs, due to the grid resolution. From sampling considerations, in a direction aligned with one of the coordinate axes, the grid is capable of supporting wavelengths greater than $2X$, corresponding to a wavenumbers of magnitude less than π/X, or frequencies $f_{trans} = \omega_{trans}/2\pi$ less than

$$f_{trans} = \frac{c}{2X} = \frac{\lambda f_s}{2}. \quad (12)$$

Above this frequency, for a simulation over a fixed volume, the solution is unreliable, as the modal density will be incorrect. See Fig. 1.

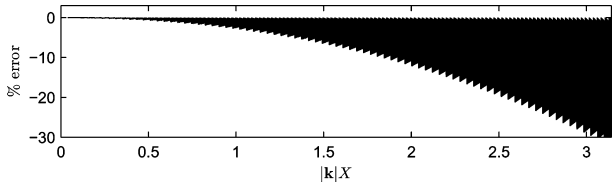

Fig. 2. Range of variation of relative phase velocity, for scheme (4), as a function of normalized wavenumber, over all directions, and expressed as a percentage error.

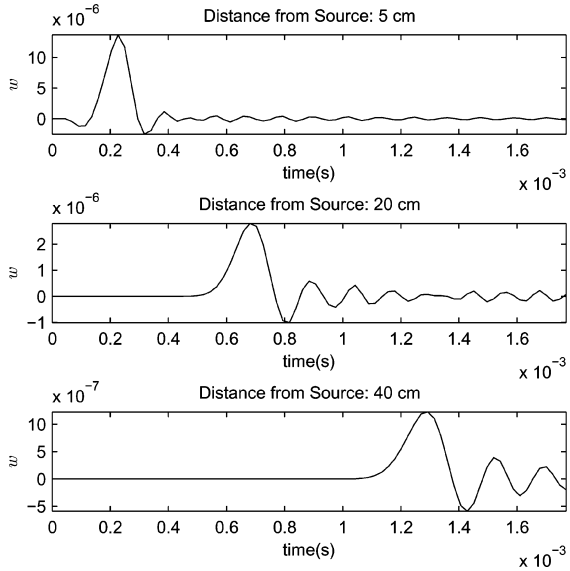

Fig. 3. Numerical dispersion, evident in the propagation of a pulse. The scheme is excited with a short pulse, of the form of a raised cosine function, at a source location, and outputs are read at successively distant locations.

This condition implies that for an FDTD scheme to give a good approximation over the entire frequency range, one must have $\lambda \geq 1$, but such a choice is prohibited by the stability condition for scheme (4), from (10).

C. Numerical Dispersion

Scheme (4) exhibits rather severe numerical dispersion, and anisotropy; waves do not travel at the same speed at all frequencies, and in all directions. In order to examine this feature, it is useful to define the relative phase velocity, as

$$v_{rel}(\mathbf{k}X) = \frac{\omega}{c|\mathbf{k}|} = \frac{2}{\lambda|\mathbf{k}X|}\sin^{-1}\left(\frac{\lambda\sqrt{\hat{\alpha}_{1,0,0}}}{2}\right) \quad (13)$$

which depends on the normalized wavenumber $\mathbf{k}X$.

In Fig. 2, the range of variation of v_{rel} with normalized wavenumber magnitude is shown—the scheme exhibits a progressive slowing of wave speed with increased wavenumber magnitude, up to a maximum of up of more than 30% at the maximum wavenumber. Such behavior is easily visible in plots of the propagation of an impulsive disturbance at increasing distances from the source location, even over short distances, as illustrated in Fig. 3.

Anisotropy also increases strongly with wavenumber, as is readily visible in Fig. 2. For plane waves, speeds range from exact (along diagonal directions on the computational grid) to maximally dispersive (along the coordinate axes). See Fig. 4, showing the variation in the form of a received pulse at three equidistant points, in distinct directions, from the source location.

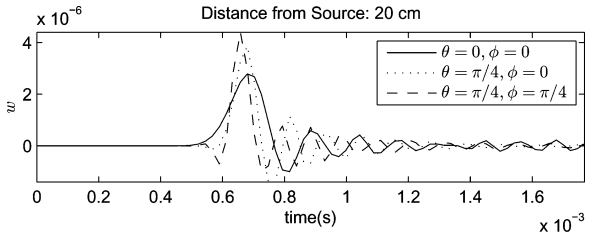

Fig. 4. Numerical anisotropy. For the same conditions as in Fig. 3, outputs are read at equidistant locations, at angles θ, ϕ relative to the positive x axis, as indicated above.

D. Comments

Scheme (4) has the virtue of simplicity; as shown above, however, it exhibits rather poor behaviour, both in terms of dispersion, and anisotropy. Various improvements are possible—all of which incur a cost, in terms of memory usage or operation count. Anistropy has been attacked using so-called interpolated schemes [9], [12], making use of a neighborhood of 27 points surrounding a given grid point, leading to nearly isotropic behavior; frequency warping techniques (necessarily offline) may be used in order to correct for dispersion error [13]. Another approach has been to make use of implicit schemes [14], [15]—while leading to greatly improved dispersion error, such schemes necessarily require linear system solutions at each time step. Many such solution techniques are available, but will either require a great increase in the operation count (as for, e.g., iterative methods which may require many iterations to converge), or are inherently serial (such as, e.g., the Thomas algorithm used for sparse banded systems [16]).

In the remainder of this correspondence, wider stencil families of explicit schemes will be explored—such schemes incur no additional cost in terms of memory, though the operation count per grid point becomes higher; but if such schemes are designed such that they possess good accuracy over the entire frequency range, it is possible to use them even at very low sampling rates (such as 4 kHz), without inducing the severe dispersive effects.

IV. Parameterized Family of Schemes

The scheme (4) operates, locally, by making use of previously computed values at the nearest neighbor points only. In this section, a framework for designing schemes which operate over an arbitrary range of neighboring points is developed.

A. Approximations to the Laplacian

Basic operations, in a finite difference scheme operating over a regular grid in 3-D are the unit shifts e_x, e_y and e_z:

$$\begin{aligned} e_x w^n_{l,m,p} &= w^n_{l+1,m,p} \\ e_y w^n_{l,m,p} &= w^n_{l,m+1,p} \\ e_z w^n_{l,m,p} &= w^n_{l,m,p+1}. \end{aligned}$$

Symmetric averaging operators, useful for isotropic problems such as the wave equation, may be defined, in terms of these basic shifts, as

$$\mu^{(b)}_\nu = \frac{1}{2}\left(e^b_\nu + e^{-b}_\nu\right) = 1 + \frac{b^2X^2}{2}\frac{\partial^2}{\partial\nu^2} + O(X^4) \tag{14}$$

where ν is any of x, y, or z, and where e^b_ν is an integer power of the shift operator in direction ν, for $b \geq 0$.

Consider the following operators, indexed by integer triplets (q, r, s), with $q \geq r \geq s \geq 0$:

$$\alpha_{q,r,s} = \frac{1}{q^2+r^2+s^2} \sum_{q',r',s'} \left(1 - \mu^{(q')}_x \mu^{(r')}_y \mu^{(s')}_z\right) \tag{15}$$

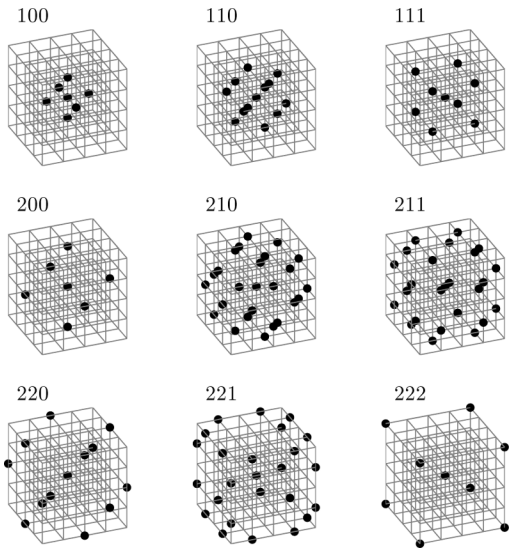

Fig. 5. Representation of the operators $\alpha_{p,q,r}$, with black points indicating the selected grid points, as for given triplet (p, q, r), up to a maximum order of $p = 2$.

where the sum is over the six permutations (q', r', s') of (q, r, s) (which are not necessarily distinct). Such an operator, when applied at a given grid point, selects the family of points distant by q, r, and s units in the three coordinate directions—see Fig. 5. In particular, the leading index q gives the maximum span of the operator in any of the three coordinate directions.

The operators

$$\delta_{q,r,s} = -\frac{1}{X^2}\alpha_{q,r,s} = \Delta + O(X^2) \tag{16}$$

are approximations to the Laplacian as may be easily verified through insertion of (14) in (15).

It follows that any linear combination of operators, where the coeficients sum to unity, is also an approximation to the Laplacian

$$\delta_{\mathbf{Q}} = \sum_{(q,r,s)\in\mathbf{Q}} \gamma_{q,r,s}\delta_{q,r,s}, \qquad \sum_{(q,r,s)\in\mathbf{Q}} \gamma_{q,r,s} = 1. \tag{17}$$

When applied at a grid point in a difference scheme, each individual operator $\delta_{q,r,s}$ selects a distinct set of six, eight, or twelve points, depending on the values of q, r, and s, as well as the center location which is common to all operators; furthermore, any grid point may be reached through the range of precisely one such operator. This particular decomposition of a general Laplacian operator over a grid is useful, in the sense that there is a direct computational cost (in terms of floating-point operations) associated with each $\delta_{q,r,s}$.

Simple families of interest include those operators which act over a given maximum number of shifts in any coordinate direction, and may be labeled as $\delta_{\mathbf{Q}_1}$, $\delta_{\mathbf{Q}_2}$, $\delta_{\mathbf{Q}_3}$, etc., where

$$\mathbf{Q}_\beta = \{(q, r, s) | q = \beta \geq r \geq s \geq 0\}. \tag{18}$$

In the spatial frequency domain, such operators can again be examined in terms of their action on a wave-like solution of the form given in (7), leading to

$$\alpha_{q,r,s} \Longrightarrow \hat{\alpha}_{(q,r,s)} = \frac{1}{q^2+r^2+s^2} \sum_{q',r',s'} (1 - c_{q',x}c_{r',x}c_{s',z}) \tag{19}$$

where $c_{\beta,\nu} = \cos(\beta k_\nu X)$ and where the approximations to the Laplacian, in the frequency domain, may be written as

$$\hat{\delta}_{q,r,s} = -\frac{1}{X^2}\hat{\alpha}_{q,r,s}. \tag{20}$$

B. Isotropy Constraints

In order to examine the isotropy of this family of schemes, it is necessary to associate power series expansions of powers of the Laplacian operator, in the frequency domain, with expansions of the parameterized operators $\delta_{\mathbf{Q}}$. To this end, note that through the use of the multinomial expansion, one may write

$$\begin{aligned}\hat{\Delta}^m &= (-1)^m \left(k_x^2 + k_y^2 + k_z^2\right)^m \\ &= (-1)^m \sum_{\zeta_x,\zeta_y,\zeta_z} \frac{m!}{\zeta_x!\zeta_y!\zeta_z!} k_x^{2\zeta_x} k_y^{2\zeta_y} k_z^{2\zeta_z} \end{aligned} \tag{21}$$

where the sum is over non-negative integers ζ_x, ζ_y, ζ_z such that $\zeta_x + \zeta_y + \zeta_z = m$.

The operator $\delta_{q,r,s}$, may be written, in the frequency domain, as

$$\hat{\delta}_{q,r,s} = \sum_{m=1}^{\infty} X^{2(m-1)} \hat{\delta}_{q,r,s}^{(m)} \tag{22}$$

where $\hat{\delta}_{q,r,s}^{(m)}$ is given by

$$\begin{aligned}\hat{\delta}_{q,r,s}^{(m)} = &\frac{(-1)^m}{q^2+r^2+s^2} \\ &\times \sum_{\zeta_x,\zeta_y,\zeta_z} \frac{k_x^{2\zeta_x} k_y^{2\zeta_y} k_z^{2\zeta_z}}{(2\zeta_x)!(2\zeta_y)!(2\zeta_z)!} \sum_{\zeta_x',\zeta_y',\zeta_z'} q^{2\zeta_x'} r^{2\zeta_y'} s^{2\zeta_z'} \end{aligned} \tag{23}$$

where the non-negative integers ζ_x, ζ_y, ζ_z satisfy $\zeta_x + \zeta_y + \zeta_z = m$, and where the second sum is over the six permutations ζ_x', ζ_y', ζ_z' of ζ_x, ζ_y, ζ_z.

Consider now a parameterized operator $\delta_{\mathbf{Q}}$, as defined in (17). In the frequency domain, such an operators may be written as

$$\begin{aligned}\hat{\delta}_{\mathbf{Q}} &= \sum_{m=1}^{\infty} X^{2(m-1)} \hat{\delta}_{\mathbf{Q}}^{(m)} \qquad \text{where} \\ \hat{\delta}_{\mathbf{Q}}^{(m)} &= \sum_{(q,r,s)\in\mathbf{Q}} \gamma_{q,r,s} \hat{\delta}_{q,r,s}^{(m)}\end{aligned}$$

For isotropy, to $2M$th order, the requirement is thus that

$$\hat{\delta}_{\mathbf{Q}}^{(m)} = g^{(m)} \Delta^m \qquad 1 \le m \le M \tag{24}$$

for some constants $g^{(m)}$. This leads to the constraints

$$\begin{aligned}\sum_{(q,r,s)\in\mathbf{Q}} &\frac{\gamma_{q,r,s}\zeta_x!\zeta_y!\zeta_z!}{(q^2+r^2+s^2)(2\zeta_x)!(2\zeta_y)!(2\zeta_z)!} \sum_{\zeta_x',\zeta_y',\zeta_z'} q^{2\zeta_x'} r^{2\zeta_y'} s^{2\zeta_z'} \\ &= g^{(m)} m! \end{aligned} \tag{25}$$

for non-negative integers $\zeta_x+\zeta_y+\zeta_z = m$, and for $m = 1, \ldots, M$. By symmetry considerations, there are $M(M-1)/2$ of such constraints, which are linear in the coefficients $\gamma_{q,r,s}$. The cardinality of the set $\mathbf{Q}$ of independent approximations to the Laplacian must thus be at least $1 + M(M-1)/2$, when the additional necessary constraint (17) is specified. Notice that the exact values of the constants $g^{(m)}$ are immaterial, as far as the constraints above are concerned.

In Sections V and VI, if a scheme is of maximal width β, and of order of isotropy α, the (possibly constrained) difference approximation to the Laplacian will be referred to as $\delta_{\mathbf{Q}_\beta^{(\alpha)}}$.

C. Family of Schemes

For a given parameterized approximation $\delta_{\mathbf{Q}}$ to the Laplacian, where the parameters satisfy constraint (17), a family of schemes may be written as

$$\delta_{tt} w_{l,m,p}^n = c^2 \delta_{\mathbf{Q}} w_{l,m,p}^n. \tag{26}$$

The stability of this family of schemes, which are explicit and two-step, may be examined again through the use of a traveling wave ansatz of the form of (7), giving rise to a characteristic equation of the form

$$\sin^2\left(\frac{\omega T}{2}\right) = \frac{\lambda^2}{4} \hat{\alpha}_{\mathbf{Q}}. \tag{27}$$

Stability conditions or the scheme are thus

$$\hat{\alpha}_{\mathbf{Q}}(\mathbf{k}X) \ge 0 \qquad \lambda \le \lambda_{\mathbf{Q}}^* = \frac{2}{\sqrt{\hat{\alpha}_{\mathbf{Q}}^{(\max)}}} \tag{28}$$

where $\hat{\alpha}_{\mathbf{Q}}^{(\max)}$ is the maximum value of the function $\hat{\alpha}_{\mathbf{Q}}$ over all possible wavenumbers, in the range $0 \le |k_x X|, |k_y X|, |k_z X| \le \pi$. The second stability constraint is strongly nonlinear in the coefficients $\gamma_{q,r,s}$. As in the case of the simple scheme, there will be substantial loss of bandwidth if λ is chosen away from the bound in (28).

The relative numerical phase velocity is

$$v_{\mathbf{Q},rel}(\mathbf{k}X, \lambda) = \frac{\omega}{c|\mathbf{k}|} = \frac{2}{\lambda|\mathbf{k}X|} \sin^{-1}\left(\lambda\sqrt{\frac{\hat{\alpha}_{\mathbf{Q}}}{2}}\right). \tag{29}$$

If the Courant number is chosen so as to satisify the stability condition (28) with equality, then the form above may be specialized to

$$v_{\mathbf{Q},rel}^*(\mathbf{k}X) = \frac{\omega}{c|\mathbf{k}|} = \frac{\sqrt{\hat{\alpha}_{\mathbf{Q}}^{(\max)}}}{|\mathbf{k}X|} \sin^{-1}\left(\sqrt{\frac{\hat{\alpha}_{\mathbf{Q}}}{\hat{\alpha}_{\mathbf{Q}}^{(\max)}}}\right). \tag{30}$$

D. Optimization

The schemes above depend on a number of free parameters (the coefficients $\gamma_{q,r,s}$), which are constrained due to the consistency condition (17), the stability conditions (28), as well as (possibly) the isotropy conditions (25). As such, optimization is necessary; optimization for FDTD schemes in the context of electromagnetics has been addressed recently in [17] and [18]. In this case, it is rather difficult to even pose the optimization problem in such a way that all schemes are on an equal footing, computationally.

The simplest approach is certainly to set the value of the Courant number $\lambda = \lambda_0$, *a priori*. Thus, the search will be over schemes of the same grid spacing (for a given sample rate), and memory requirements are identical over the search space. In order to ensure that there is no region of the spectrum over which modal density is incorrect, as per the discussion in Section III-B, one can go further and specify $\lambda_0 \ge 1$ (and preferably, for reasons of efficiency, $\lambda_0 \cong 1$). All of the constraints are thus linear, and the optimization problem is greatly simplified.

On the other hand, such an approach neglects the natural tendency of all such schemes to have the least numerical dispersion (and maximal output bandwidth) when the Courant number is chosen close to the stability condition; there is also no guarantee that such a scheme will be stable, as the second of conditions (28) may not be respected. As such, the approach taken here will be to set the Courant number, *a priori*, to its maximum value, for a given set of coefficients. There is thus the possibility of some variation in λ, and thus memory requirements, though as will be shown below, in practice, the optimal scheme nearly always takes on a value of λ near to unity (in fact, near 0.9).

A simple choice of the objective function is the mean square deviation of the relative phase velocity of the scheme, integrated over the positive octant of wavenumber space:

$$E_{\mathbf{Q}} = \int_{|\mathbf{k}X|\le\pi} \left(v_{\mathbf{Q},rel}^* - 1\right)^2 d\mathbf{k}X \tag{31}$$

and the optimal set of parameters $\gamma_{q,r,s}$, for a given family $\mathbf{Q}$ of schemes may be recovered as

$$\gamma_{q,r,s}^{(opt)} = \arg\min\left(E_{\mathbf{Q}}\right) \tag{32}$$

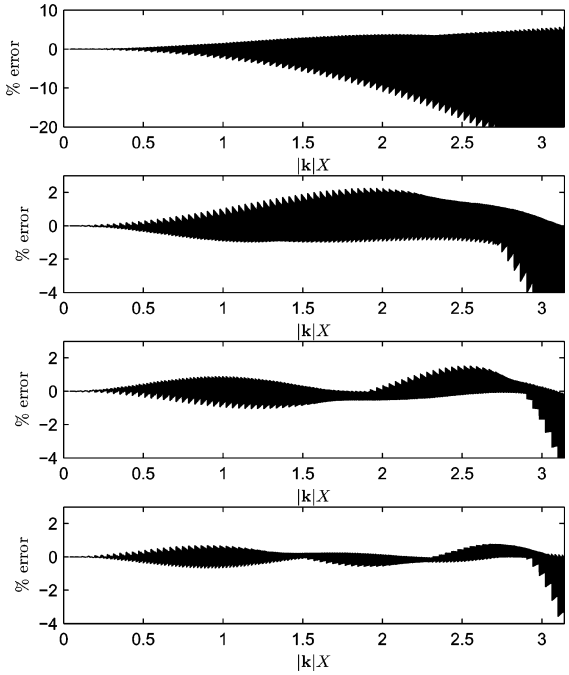

Fig. 6. Range of variation of relative phase velocity, as a function of normalized wavenumber, over all directions, and expressed as a percentage error. From top to bottom, for the optimal successively wider stencil schemes defined over sets of points $\mathbf{Q}_1$, $\mathbf{Q}_2$, $\mathbf{Q}_3$, and $\mathbf{Q}_4$.

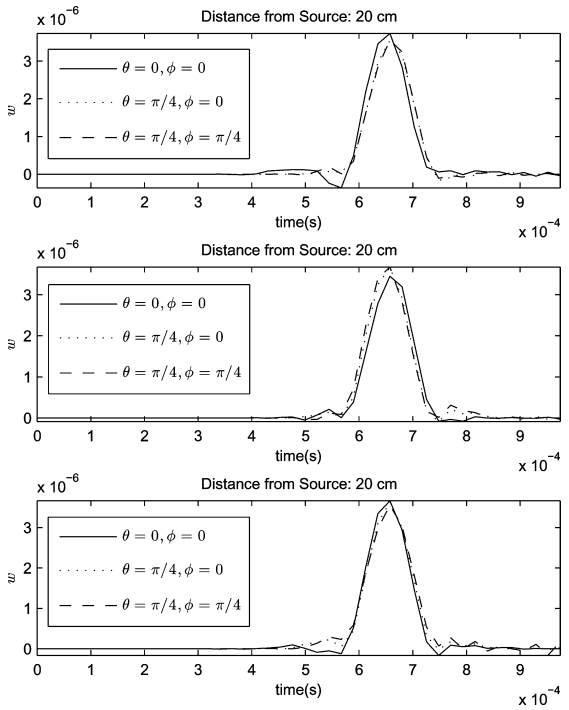

Fig. 7. Numerical anisotropy. For the conditions in Fig. 3, outputs are read at equidistant locations, at angles θ, ϕ relative to the positive x axis, as indicated above. Shown are results for the optimal schemes $\mathbf{Q}_2$, $\mathbf{Q}_3$, and $\mathbf{Q}_4$.

for $(q, r, s) \in \mathbf{Q}$, subject to consistency and isotropy constraints.

It is not the purpose of this correspondence to detail optimization techniques, of which there is of course a vast number—see, e.g., [19] for basic strategies. All optimization results illustrated in Section V are obtained using simple gradient descent methods, accompanied by line searches.

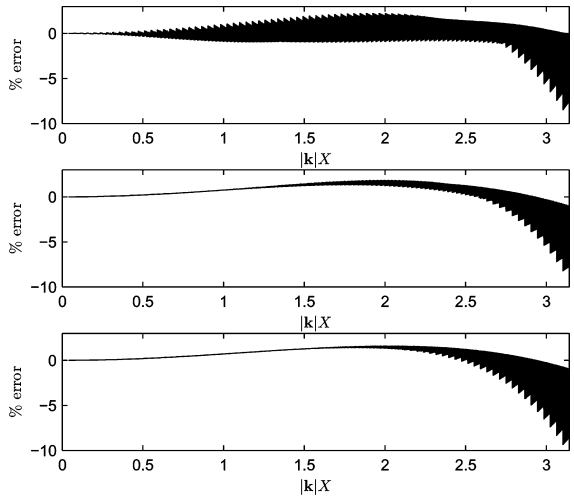

Fig. 8. Range of variation of relative phase velocity, as a function of normalized wavenumber, over all directions, and expressed as a percentage error. From top to bottom, for the optimal successively more isotropic schemes defined over sets of points $\mathbf{Q}_2^{(2)}$, $\mathbf{Q}_2^{(4)}$, and $\mathbf{Q}_2^{(6)}$.

V. Numerical Results

In this section, numerical results, including both plots of variation is numerical phase velocity, as well as time domain results of the use of the schemes are presented. In the latter case, all schemes are run at a sample rate of 44.1 kHz; an impulsive input waveform, of the form of a raised cosine function of duration eight samples is applied at a given grid location, and output is drawn from other locations (interpolated spatially using high-order 3-D sinc functions).

Consider first the optimal schemes $\mathbf{Q}_1$, $\mathbf{Q}_2$, $\mathbf{Q}_3$, and $\mathbf{Q}_4$, of successively larger stencil width. Plots of variation of relative numerical phase velocity are shown in Fig. 6, as a function of normalized wavenumber magnitude. Though error is always largest near the spatial Nyquist frequency (i.e., when $|\mathbf{k}X| = \pi$), it is noticeably reduced for the higher stencil schemes; for scheme $\mathbf{Q}_4$, it is under 1% over nearly the entirety of the range of wavenumbers. The values of the Courant number, for the four optimal schemes, are

$$\lambda_{\mathbf{Q}_1} = 0.69 \quad \lambda_{\mathbf{Q}_2} = 0.87 \quad \lambda_{\mathbf{Q}_3} = 0.89 \quad \lambda_{\mathbf{Q}_1} = 0.89 \qquad (33)$$

and thus the range of wavenumbers over which modal density is incorrect is small (see Section III-B). Plots of the propagation of short pulses at three propagation angles are shown in Fig. 7, which is to be compared with the results of the simple scheme in Fig 4; as expected, coherence of the pulse is much higher.

Consider now schemes of a fixed stencil width, constrained to different orders of isotropy, such as the schemes $\mathbf{Q}_2^{(1)}$, $\mathbf{Q}_2^{(2)}$, and $\mathbf{Q}_2^{(3)}$. The variation in phase velocity with direction, as shown in Fig. 8, is virtually negligible over the majority of the range of wavenumbers, though there is now evident a general offset of phase velocity, uniform over all directions. The optimal values of the Courant number, in this case, are

$$\lambda_{\mathbf{Q}_2^{(1)}} = 0.87 \qquad \lambda_{\mathbf{Q}_2^{(2)}} = 0.90 \qquad \lambda_{\mathbf{Q}_2^{(3)}} = 0.89. \qquad (34)$$

With the exception of the highest wavenumbers, propagation of even a sharp pulse is nearly entirely independent of direction, as seen in Fig. 9.

VI. Conclusion and Future Directions

It has been shown here that there are opportunities for improvement of FDTD methods in acoustic simulation, at the level of algorithm design, with respect to various criteria. The main interest of the schemes presented here is that programming simplicity and memory

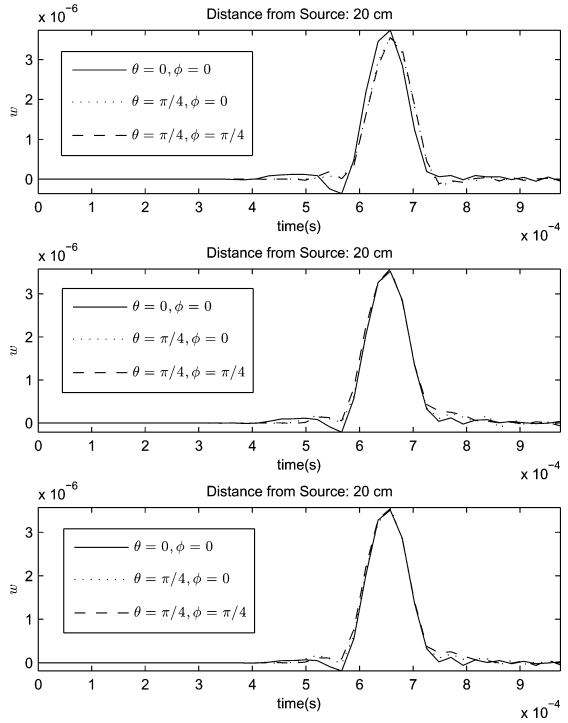

Fig. 9. For the conditions in Fig. 3, outputs are read at equidistant locations, at angles θ, ϕ relative to the positive x axis, as indicated above. Shown are results for the optimal schemes $\mathbf{Q}_2^{(2)}$, $\mathbf{Q}_2^{(4)}$, and $\mathbf{Q}_2^{(6)}$.

requirements are unchanged relative to that of the simple scheme presented in Section III, though the operation count is certainly higher; such schemes perform very well even at low audio sample rates. Only the behavior of schemes over the problem interior has been addressed here. Necessary further steps are to specialize such schemes to numerical boundary conditions typical of room acoustics problems (see, e.g., [20]). Maintaining numerical stability for wider stencil schemes may be a strenuous task, but theoretical tools are available for such schemes [21].

The optimization problem described in Section IV-D has been defined in the simplest possible manner, and could be fine tuned in a great variety of ways. Regarding the objective function given in (31)—as seen in the plots of variation in relative phase velocity for optimal schemes, as appear in Section V, as most of the error is near the highest wavenumbers supported on the grid, it might be beneficial to accept such error as unavoidable, perhaps through the introduction of a weighting in the objective function, or perhaps performing the optimization only over a selected region of wavenumber space (leaving a "guard band") near the highest wavenumbers. Isotropy constraints, in this correspondence, are posed in the classical numerical sense of Taylor series expansions about DC (much as in the case of conventional analysis of accuracy of finite difference schemes [11]). One could, instead of dealing with isotropy directly through constraints, build it in directly to the objective function, in a wideband sense, such that variation of the relative phase velocity is minimized for a given value of the wavenumber magnitude. There are many other features of interest in audio and numerical design which could also be built into the above optimization strategy as additional constraints. Among them are: the possibility of minimizing the variation of relative phase velocity at the highest wavenumbers (thus targeting spurious oscillation near the Nyquist frequency); accuracy as a whole, in the classical numerical sense, which may be raised from second order through new constraints on the Courant number, using modified equation methods [22].

REFERENCES

[1] T. Funkhouser *et al.*, "A beam tracing method for interactive architectural acoustics," *J. Acoust. Soc. Amer.*, vol. 115, no. 2, pp. 739–756, 2004.

[2] J. Allen and D. Berkley, "Image method for efficiently simulating small-room acoustics," *J. Acoust. Soc. Amer.*, vol. 65, no. 4, pp. 943–950, 1979.

[3] D. Botteldooren, "Finite-difference time-domain simulation of low-frequency room acoustic problems," *J. Acoust. Soc. Amer.*, vol. 98, no. 6, pp. 3302–3308, 1995.

[4] L. Savioja, T. Rinne, and T. Takala, "Simulation of room acoustics with a 3-D finite-difference mesh," in *Proc. Int. Comp. Music Conf.*, Arhus, Denmark, Sep. 1994, pp. 463–466.

[5] D. Murphy, A. Kelloniemi, J. Mullen, and S. Shelley, "Acoustic modelling using the digital waveguide mesh," *IEEE Signal Process. Mag.*, vol. 24, no. 2, pp. 55–66, Mar. 2007.

[6] L. Savioja, J. Backman, A. Järvinen, and T. Takala, "Waveguide mesh method for low-frequency simulation of room acoustics," in *Proc. 15th Int. Conf. Acoust.*, Trondheim, Norway, Jun. 1995, pp. 637–640.

[7] M. Beeson and D. Murphy, "Roomweaver: A digital waveguide mesh based room acoustics research tool," in *Proc. 7th Int. Digital Audio Effects Conf.*, Naples, Italy, Oct. 2004, pp. 268–273.

[8] D. Murphy, M. Beeson, S. Sheeley, and A. Moore, "Hybrid room impulse response synthesis in digital waveguide mesh," in *Proc. 11th Int. Digital Audio Effects Conf.*, Espoo, Finland, Sep. 2008.

[9] S. Bilbao, *Wave and Scattering Methods for Numerical Simulation*. Chichester, U.K.: Wiley, 2004.

[10] P. Morse and U. Ingard, *Theoretical Acoustics*. Princeton, NJ: Princeton Univ. Press, 1968.

[11] J. Strikwerda, *Finite Difference Schemes and Partial Differential Equations*. Pacific Grove, CA: Wadsworth and Brooks/Cole Advanced Books and Software, 1989.

[12] K. Kowalczyk and M. van Walstijn, "Room acoustics simulation using 3-d compact explicit fdtd schemes," *IEEE Trans. Audio, Speech, Lang. Process.*, vol. 19, no. 1, pp. 34–46, Jan. 2011.

[13] L. Savioja and V. Välimäki, "Interpolated rectangular 3-d digital-waveguide mesh algorithms with frequency warping," *IEEE Trans. Speech Audio Process.*, vol. 1, no. 6, pp. 738–790, Jan. 2003.

[14] K. Kowalczyk and M. van Walstijn, "A comparison of nonstaggered compact FDTD schemes for the 3D wave equation," in *Proc. IEEE Int. Conf. Acoust., Speech, Signal Process.*, Dallas, TXs, Mar. 2010, vol. 4, pp. 197–200.

[15] S. Bilbao, "Parameterized families of finite difference schemes for the wave equation," *Numer. Meth. for Partial Different. Equat.*, vol. 20, no. 3, pp. 463–480, 2004.

[16] Y. Zhang, J. Cohen, and J. D. Owens, "Fast tridiagonal solvers on the gpu," in *Proc. 15th ACM SIGPLAN Symp. Principles Practice of Parallel Prog.*, New York, 2010, pp. 127–136, PPoPP '10.

[17] T. Zygiridis and T. Tsiboukis, "Design of optimized FDTD schemes for the accurate," *IEEE Trans. Magn.*, vol. 42, no. 4, pp. 811–814, Apr. 2006.

[18] S. Wang and F. Teixeira, "Grid-dispersion error reduction for broadband," *IEEE Trans. Magn.*, vol. 40, no. 2, pp. 1440–1443, Mar. 2004.

[19] E. Chong and S. Zak, *An Introduction to Optimization*, third ed. Hoboken, NJ: Wiley, 2008.

[20] K. Kowalczyk and M. van Walstijn, "Modeling frequency-dependent boundaries as digital impedance filters in FDTD and K-DWMroom acoustics simulations," *J. Audio Eng. Soc.*, vol. 56, no. 7/8, pp. 569–583, 2008.

[21] H.-O. Kreiss, N. Petersson, and J. Yström, "Difference approximations for the second order wave equation," *SIAM J. Numer. Anal.*, vol. 40, no. 5, pp. 1940–1967, 2003.

[22] G. R. Shubin and J. B. Bell, "A modified equation approach to constructing fourth order methods for acoustic wave propagation," *SIAM J. Sci. Statist. Comput.*, vol. 8, pp. 135–151, 1987.